1-1-1972

Measurements Program in Remote Sensing

Leroy F. Silva

Information Note 012872

MEASUREMENTS PROGRAM IN REMOTE SENSING AT PURDUE UNIVERSITY

by

LeRoy F. Silva and Staff

Laboratory for Applications of Remote Sensing (LARS)

Purdue University

West Lafayette, Indiana

Presented at the Fourth Annual Earth Resources Program Review, Manned Spacecraft Center (NASA), Houston, Texas, January 17, 1972.

MEASUREMENTS PROGRAM IN REMOTE SENSING AT PURDUE UNIVERSITY *

by

LeRoy F. Silva and Staff
Laboratory for Applications of Remote Sensing (LARS)
Purdue University
West Lafayette, Indiana

INTRODUCTION

The measurements program at LARS/Purdue has been concerned with five basic research areas during 1971. These areas are (1) the influence of haze layers upon remotely sensed surface properties, (2) electrical methods of soil moisture measurement, (3) thermographic studies of vegetation under nutritional stress, (4) improved field spectroradiometry, and (5) biological spectrophotometry.

All of these projects have risen out of problems generated from the overall laboratory mission. The emphasis in this paper is on instrumentation and techniques; whereas, related data and results on specific projects will be reported elsewhere. Each of the subject areas will be discussed individually.

INFLUENCE OF HAZE LAYERS ON REMOTELY SENSED SURFACE PROPERTIES

During the analysis of data gathered for the 1971 Corn Blight Watch Experiment a number of unexpected features were observed. One of particular interest was the appearance of bright and dark sides along the flightline of the aircraft. An example is shown in Figure 1, taken at 10:28 a.m. EST on June 30, 1971, over southern Indiana. The plane was headed south (top of figure) with surface illumination from the east (left) and ahead of the plane. Relative darkness on the left and bright-

* In this paper, results from a number of studies are summarized; researchers are identified in the acknowledgment section.

ness on the right is evident in the data as it appeared when displayed in digitized grey levels.

A check of the pilot's log revealed that visibility was estimated to be only 6 miles while hazy conditions were noted below the aircraft. The possibility that the presence of hazy layers may have contributed to the anomalous effects in the data prompted the computation of scattering angles for this flight. These are shown in Figure 2. The scattering angle varies from near side-scattering on the left (east) side of the flightline to near back-scattering on the right (west) side. Since the scattering properties of the aerosols which compose haze layers generally undergo marked variations over this range of scattering angles (Deirmendjian, 1969), an attempt to compute the expected variation of reflected intensities across the flightline was made. It was first necessary to assign physical parameters to the haze. As a first case, the size distribution of Deirmendjian's haze L (Deirmendjian, 1969) was selected as being typical of a continental-type aerosol distribution. His tabulations of the elements of the scattering matrix for a water haze L allowed the computation of the scattering phase function for the scattering angle interval of interest. This function, shown in Figure 3, for a wavelength of 0.45 micrometers undergoes a minimum near 120° from which it rises to a relative maximum at 165° with a secondary minimum between this point and the maximum value for 180° backscatter.

Combination of the computed scattering angles of Figure 2 with the phase function in Figure 3 allowed an estimate to be made of the variation in reflected intensity across the flightline. The result for a wavelength of 0.45 micrometers is presented in Figure 4 as the predicted curve. Lowest values occur along the left (east) side of the flightline. These correspond to minimum values of the scattering phase function near 120°. As scattering angles increase moving to the right (west) intensity increases reaching a peak for 165° scattering angle. Beyond this point the reflected intensity decreases toward the right-hand side of the flightline.

In order to obtain a measure of the agreement between these calculations and the observed intensities, the latter were averaged column-by-column for the total length of the flightline. The resultant values, computed for the 0.46 - 0.49 spectral interval, are shown as the observed curve in Figure 4. The agreement between the two curves is excellent for the left-hand side of the flightline, but differences as large as 30 percent occur near the right-hand side. At the present time, no satisfactory explanation exists for this discrepancy.

Although the agreement for this case between theory and observations is far from perfect, the results are sufficiently encouraging to warrant further study. At the present time, a model of atmospheric attenuation (Elterman, 1970) is being adapted for application to problems of this nature. The Elterman model consists of tabulations of attenuation coefficients at various wavelengths from 0.27 to 4.00 micrometers for several altitudes from the surface to 50 kilometers. The attenuation coefficients account for Rayleigh scattering, ozone, and aerosol extinction in the atmosphere. The manner in which the presence of a haze layer might be included in such a standard model is shown in Figure 5. In addition to reducing the radiation which reaches the surface and is reflected to the aircraft, the haze layer contributes a component through multiple internal scattering. As a result of the combination of these two factors, the spectral nature of the radiation received at the aircraft can be modified. It is hoped that it will eventually be possible to represent the haze layer by parameters such as an effective transmissivity and reflectivity. In this way it will be possible to improve the identification of surface properties from multispectral remote sensed data.

ELECTRICAL METHODS OF SOIL MOISTURE MEASUREMENT

Work on the electrical properties of soil has gone on for several decades. The electrical properties of soils are of interest for two basic reasons.

1. Can field soil moisture measurements be made more easily using some electrical technique?

2. Is it possible to extend the results of electrical measurements to remote sensing soil moisture measurement techniques?

The work of Blanchard[3] and of Rousch[4] concerning the measurement of soil moisture using microwave techniques has been reported elsewhere in these proceedings. Earlier, Davis et al[5] produced a study of the radar scattering characteristics of soils as a function of moisture content.

Purdue researchers decided to study the variation of soil permittivity; that is, a capacitance measurement versus moisture. This decision was made after an extensive literature study indicated that soil salt content strongly influenced results of techniques which depended upon conductivity measurements. The basic sample holder used is a coaxial structure in which laboratory prepared soil samples were inserted. The samples were prepared by mixing a particular soil type with ice in a

cold room and then packing the mixture into the soil sample holder. The sample holder is hermetically sealed so that the moisture content of this system remains stable after the sample holder is loaded. The sample is allowed to rise to room temperature at which time the capacitance (and conductance) of the sample holder and its contents is measured on a standard impedance bridge.

In Figure 6, the capacitance of a sample holder containing a particular soil type at a fixed percentage of moisture is measured as a function of frequency. In principle the capacitance of the sample should be frequency independant. But the presence of salts in the soil sample create free ions which form a polarization layer near the outside surface of the coaxial sample holder. This produces an effective resistance capacitance combination that appears in a series with the actual capacitance resistance combination of the soil sample itself. The capacitance of the soil sample is actually frequency independant; whereas, the capacitance of the polarization layer depends upon frequency due to ion inertia effects. In Figure 6 a theoretical curve based on a simple two-element lump capacitive model is also shown. On the same set of axes, some experimental data for a particular soil sample is also plotted. The difference between the two curves can be explained due to the simplicity of the lumped model. As more elements are inserted and the approximation to the actual distributed capacitance case is approached, one would expect experimental and calculated results to come closer together. Such modeling attempts are currently in progress.

In Figure 7a the relationship between capacitance and soil moisture for a particular soil type is plotted. Some scatter in the data is observed. However, no attempt was made during the preparation of these data to control the compaction and curing time of the sample. Curing time is defined as the period between the time the sample is loaded and the time the sample is measured. One would expect that if these two parameters were controlled that less scatter in the data would result. The important result to be derived from Figure 7 is that a definite well-defined trend does exist between soil capacitance and soil moisture. There is promise that a simple field probe based upon the principle discussed here could be developed that would simplify soil moisture measurements. The problem of extending these results to microwave measurements is considerably more involved and the question of whether a closed form solution exists to the analytical problem that is involved has yet to be determined.

THERMOGRAPHIC STUDIES OF NUTRITIONALLY STRESSED VEGETATION

A Barnes Model T-4 scanning radiometer has been used to study corn plants and leaves under several conditions of nutritional stress. Corn plants grown in a hydroponic green house experiment with controlled nutritional deficiencies were examined in a variety of environments to ascertain leaf-thermal variation. The thermogram of a sulfur deficient corn plant is shown in Figure 8. The sulfur deficient corn plant is in the left-hand portion of the figure, whereas a control healthy corn plant is in the right-hand portion of the figure. The object in the middle of the slide is a blackbody reference. The ambient temperature of this experiment was 24°C. However, the surface located immediately behind both plants was at a temperature of 16.5°C. The nutritionally stressed plant was approximately 1°C cooler than the control plant. This fact would have been difficult to ascertain with a conventional radiometer because of the thermal-spatial variations on the nutritionally stressed plant. Because of the fourth power variation of radiation with respect to temperature the warmer portions of the nutritionally stressed plant dominate the radiation of the whole plant and tend to obscure the actual thermal condition of the plant. The use of the scanning radiometer enables one to finely delineate the temperature profile of a plant when compared to a healthy controlled plant. One observes that the control plant exhibits a relatively uniform thermal-spatial variation. In Figure 9 a similar experiment involving a nitrogen deficient plant is shown. The nitrogen deficient plant exhibits approximately a 2°C cooler temperature again with a 16.5°C background reference surface and a 23°C ambient temperature. In both Figures 8 and 9 the scan time to develop the thermogram was six minutes.

In Figure 10 a thermogram of control and nutritionally stressed corn leaves is shown. From left to right the leaves are: control, three sulfur deficient leaves, a control leaf, three nitrogen deficient leaves, and another control leaf. The scan time used to develop the thermogram was 4 1/2 seconds. A styrofoam surface was used as the background for the corn leaves. A warm surface of approximately 35°C (a heating anemostat) was located near the experiment. The ambient temperature was approximately 23°C. The sulfur deficient leaves are approximately 1°C warmer; whereas, the nitrogen deficient leaves are approximately 2°C warmer than the control leaves.

The preliminary conclusion is that nutritionally stressed plants are not always hotter than a control plant, but apparently are influenced more strongly by environment. It is, therefore, possible for nutritionally stressed plants to be cooler than healthy plants in a similar environment if a cold surface is located nearby. It appears from this

experiment that nutritionally stressed plants are not as well able to control their temperature as a healthy plant in the same environmental situation. Controlled field experiments are being designed to see if this effect can be observed in a natural environment.

AN IMPROVED FIELD SPECTRORADIOMETER

Previously[6] it has been shown that it is essential to have rapid spectral scan capabilities in field spectroradiometric measurement situations. For example, in Figures 11 and 12 data taken with an SG-4 Perkin Elmer Spectroradiometer is shown. In Figure 6 it is seen that during the spectral scan period solar conditions changed which compromised the data that were being observed. To further illustrate the problems of spectral scan time, the same spectrometer was set at a particular wavelength and pointed at a corn plant. The spectrometer was located in an aerial lift system. The wobbles in the data taken at the fixed wavelength are not due to detector noise but are due to the wind disturbing the geometry of the corn plant. These effects are in addition to the appearance and disappearance of the sun due to cloud cover. Therefore, the requirement that relatively rapid spectral scans be available in field spectroradiometers was made evident.

A field spectroradiometer built to specifications developed by the USDA facility at Weslaco, Texas, Stanford University, and Purdue University was built by Exotech, Inc. of Gaithersburg, Maryland. This instrument, designated the Model 20B, has been described in detail at the Michigan Symposium of 1971.[7] In summary, the instrument featured refractive fore-optics and covered the wavelength range from .4 to .5μm and 2.8 to 15μm. Four detectors with Joule-Thompson cooling, circular variable filter wheel spectrum scanning, 1 to 30 second adjustable spectral scans and adjustable field of view from 3/4 to 15° were features of this instrument. Figure 13 shows this instrument under field trial.

Based upon field experience with this instrument, another instrument, designated the Model 20C, has been specified and built by Exotech, Inc. for LARS/Purdue. This instrument features a reflective fore-optic system (Newtonian telescopes), a field calibration system, and an in-line sighting system. In addition, several electronic improvements and an electrical view angle adjustment feature have been included.

A general view of the short wavelength head (.4μm to 2.5μm) along with its control console is shown in Figure 14. The control console is normally located in an instrument van and the operator can control scan speed, detector gain, field of view, and the viewing port inside the instrument van; the look angle and focus are controlled by an operator

located at the instrument head. A close-up of the instrument head is shown in Figure 15. The vertical tube contains a ceramic plate that approximates a Lambertian receiver so that the solar irradiance can be spectrally monitored almost simultaneously with the target radiance. The detectors are sensitive to either the solar irradiance or the target radiance, depending upon a position of a mirror within the instrument that is controlled by the operator. The view angle adjustment of the instrument is shown in Figure 16, whereas the features of the Newtonian telescope fore-optical system are illustrated in Figure 17.

The internal structure of the chopper module is shown in Figure 18. The chopper wheel, visible in the middle of the chopper module, is arranged so that each of the two detectors in the instrument head are alternately exposed to the incoming radiation and a blackbody reference located within the instrument. The circular variable filter wheels are joined together by a timing belt and are located between the detectors and a set of relay optics which focus the impinging radiation on the appropriate detector. The low noise pre-amplifiers are located in close proximity to the detectors and a carefully designed grounding system is used to minimize noise pick-up. Hall-Effect motors are used to avoid brush arcing effects. The Joule-Thompson cooling assembly is illustrated in Figure 19. Joule-Thompson coolers are used in preference to conventional liquid nitrogen cooled dewars so as to permit a wide range of instrument head operating angles. Some typical data that has been reported elsewhere[6] is shown in Figure 20.

The data from the instrument is recorded on a seven-channel analog tape recorder which is then subsequently digitized in the laboratory's analog to digital conversion system. A software system has been developed which enables the user to present the data in calibrated form in a variety of formats.

A BIOLOGICAL SPECTROPHOTOMETER

A new spectrophotometer, shown in Figure 21, designed expressly to obtain data on intact biological samples, has been recently developed. The radiation, which interacts with the specimen and is subsequently measured, is influenced by the absorption, distribution of the absorbing substances, light scattering, and geometry of the specimen. In order to quantify these factors, the primary design criterion was to develop a monochromator having high power output consistant with good quality spectra. High incident power contributes to improved spatial resolution and geometrical measurements of the radiation reflected or transmitted by the specimen as well as permitting greater freedom in the selection of the detectors.

The instrument source is a quartz iodine lamp. The lamp filament is at the focal point of the first or collimating mirror and replaces the entrance slit of a conventional monochromator design as shown in Figure 22. The lamp is water cooled and baffled in such a way that the light that enters the monochromator is restricted to that which is actually used by the optics of the system.

The primary dispersion element is a 5" x 6" defraction grading blazed at 600 nm. A linear variable-wavelength filter for order sorting and reducing stray light is located at the exit slit, and the movement of the filter is synchronized with the grading rotation. A reference cell is used to monitor the output of the monochromator.

Assemblies for measuring bi-directional reflectance and large area reflectance are shown in Figures 23 and 24. Typical data obtained from the bi-directional reflectance is shown in Figure 25 following procedures outlined by Breece and Holmes.[8]

The DC measurement system is available where the output of the detector is fed directly to an operational amplifier. Either linear or logarithmic output can be used. This system is very easy to operate and provides a means of radiation measurement for any source such as flourescence where light chopping cannot be accomplished easily. The chopped light system is also incorporated in the instrument in conjunction with a commercial lock-in amplifier and provides a lower noise equivalent power than the DC system.

Data are recorded on an XY recorder or may be recorded in digital form or subsequent digital processing. For normal use the data requires corrections for spectral response and wavelength. And the system is set up so that these corrections are subsequently made by a computer.

The performance summary of the system follows.

monochromator output power: (1000 watt lamp), 700nm, 10^{-2} watts
band pass: 10nm
wavelength range: 350 to 1200nm
scanning speed: .03nm/sec to 30nm/sec
detector noise equivalent power: 530nm
photomultiplier: 10^{-15} watts
recording-analog, XY recorder: 8 1/2" x 11"
digital paper tape, direct computer interface, record interval 10nm

The transmittance assembly capable of measuring the transmittance of fixed specimens is also included in the basic instrument structure. Transmittance spectra of specimens as thick as a grapefruit can be easily obtained on this instrument. A large reflectance assembly was designed

to provide a means for obtaining an area integrated reflectance measurement. Detector geometry can be modified to suit the experimental requirements. The bi-directional assembly was used to obtain reflectance data as a function of angle of incidence and angle of detection. The coordination of this instrument with the field spectroradiometer described in the previous section enables the researcher to develop a complete laboratory-field experimental design on many natural systems.

ACKNOWLEDGMENTS

The work described in this report represents the work of many investigators. They are as follows:

1. Influence of Haze Layers on Remotely Sensed Surface Properties
   Prof. Gerald Jurica, Mr. William Murray

2. Electrical Methods of Soil Moisture Measurement
   Prof. Floyd V. Schultz, Mr. James Zalusky

3. Thermographic Studies of Vegetation Under Nutritional Stress
   Dr. Hasan Al-Abbas, Prof. LeRoy F. Silva, Mr. Frederick L. Phillips

4. Improved Field Spectroradiometry
   Mr. Barrett Robinson, Mr. Robert Haselby, Prof. LeRoy F. Silva

5. Biological Spectrophotometry
   Dr. Gerald Birth

The work described in this paper was supported by NASA under contract #15-005-112.

REFERENCES

(1) Deirmendjian, D., 1969. Electromagnetic Scattering on Spherical Polydispersions. New York, American Elsevier Publishing Co., 290 pp.

(2) Elterman, L., 1970. Vertical-Attenuation Model with Eight Surface Meteorological Ranges 2 to 13 Kilometers. Air Force Cambridge Research Laboratories, Environmental Research Papers No. 318, Bedford, Mass., 56pp.

(3) Blanchard, B., 1972. Measurements from Aircraft to Characterize Watersheds, 4th Annual Earth Resources Program Review: NASA, Houston, Tex. Jan. 17-21, 1972.

(4) Rouse, J. A Coactive Interdisciplinary Research Program with NASA, 4th Annual Earth Resources Program Review: NASA, Houston, Tex. Jan. 17-21, 1972.

(5) Davis, B.R., J.R. Lundien, and A.N. Williamson, Jr., Feasibility Study of the Use of Radar to Detect Surface and Ground Water, Technical Report No. 3-727, U.S. Army Engineer Waterways Experiment Station, Corps of Engineers, Vicksburg, Mississippi, April, 1966.

(6) Remote Multispectral Sensing in Agriculture, Laboratory for Agricultural Remote Sensing, Volume 2 (Annual Report), p. 55, July, 1967.

(7) Silva, L., R. Hoffer, and J. Cipra, Extended Wavelength Field Spectroradiometry, Proceedings of the Seventh International Symposium on Remote Sensing of Environment, Volume II, P. 1509, May, 1971.

(8) Breece, H., III, and R. Holmes, Bidirectional Scattering Characteristics of Healthy Green Soybean and Corn Leaves in vivo, Applied Optics, Volume 12, p. 119, January, 1971.

Figure 1. Data in 0.46-0.49 micrometers channel taken from June 30, 1971, flight over Pike County, Indiana (Segment 225)

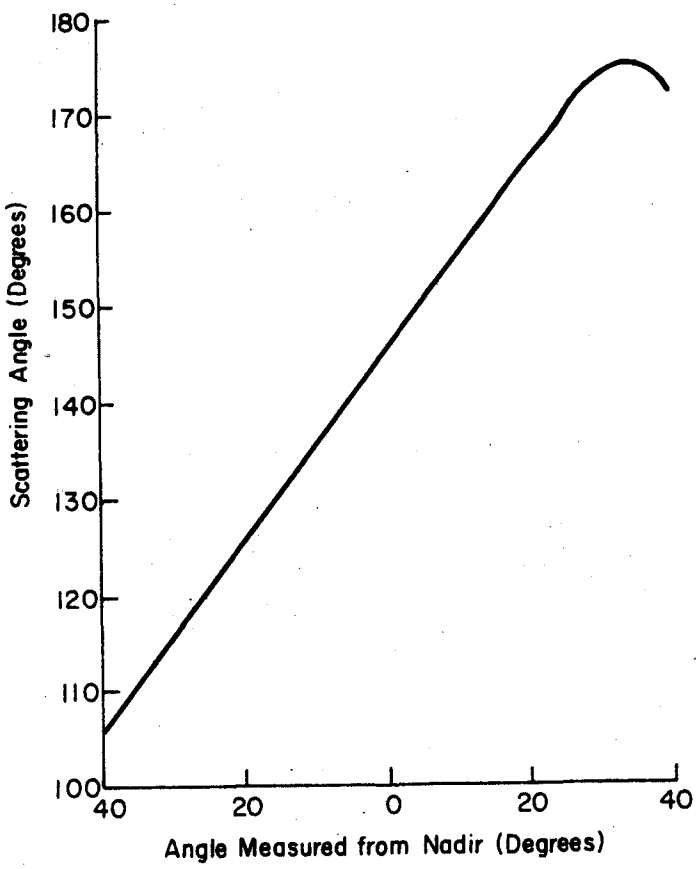

Figure 2. Scattering angles computed for June 30, 1971, flight over Segment 225.

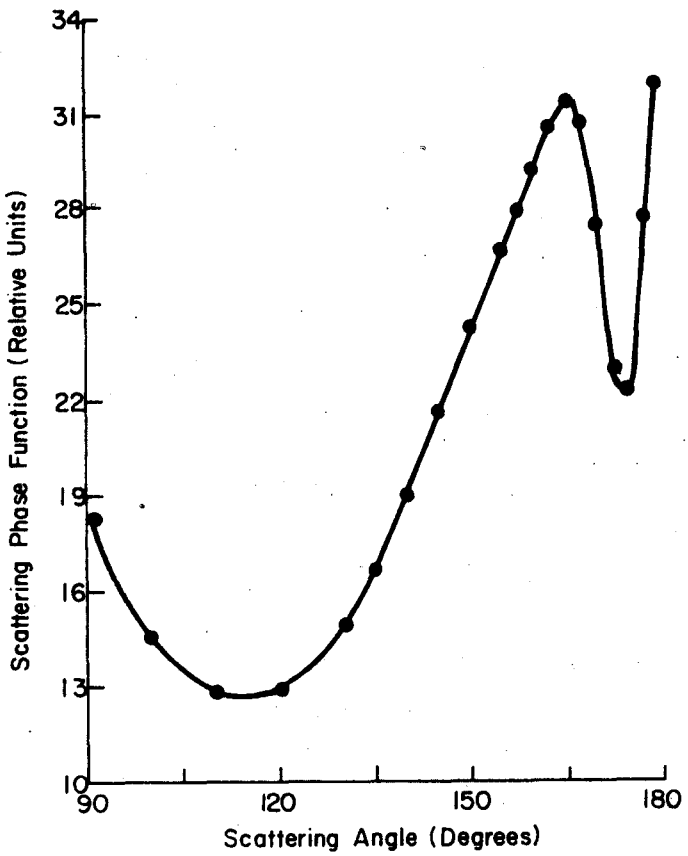

Figure 3. Scattering phase function at 0.45 micrometers as a function of scattering angle for a continental haze layer (after Deirmendjian, 1969).

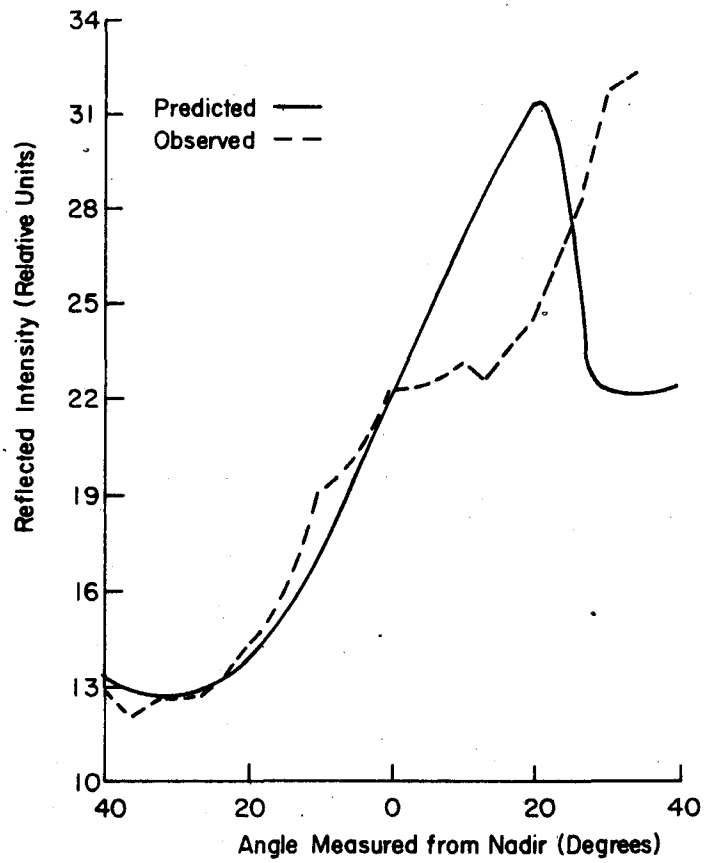

Figure 4. Comparison between predicted reflected intensity at 0.45 micrometers and observed values for 0.46-0.49 micrometers averaged for the length of the June 30, 1971, flight over Segment 225.

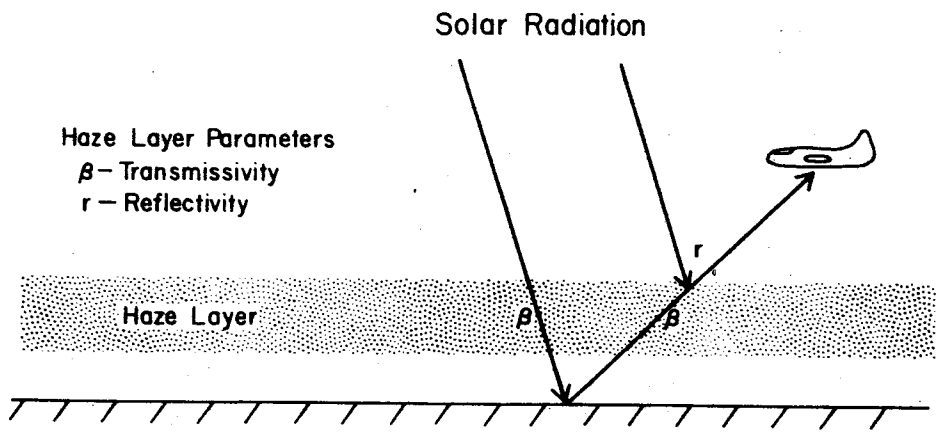

Figure 5. A schematic representation of the influence of a haze layer upon surface-reflected radiation measured from an aircraft.

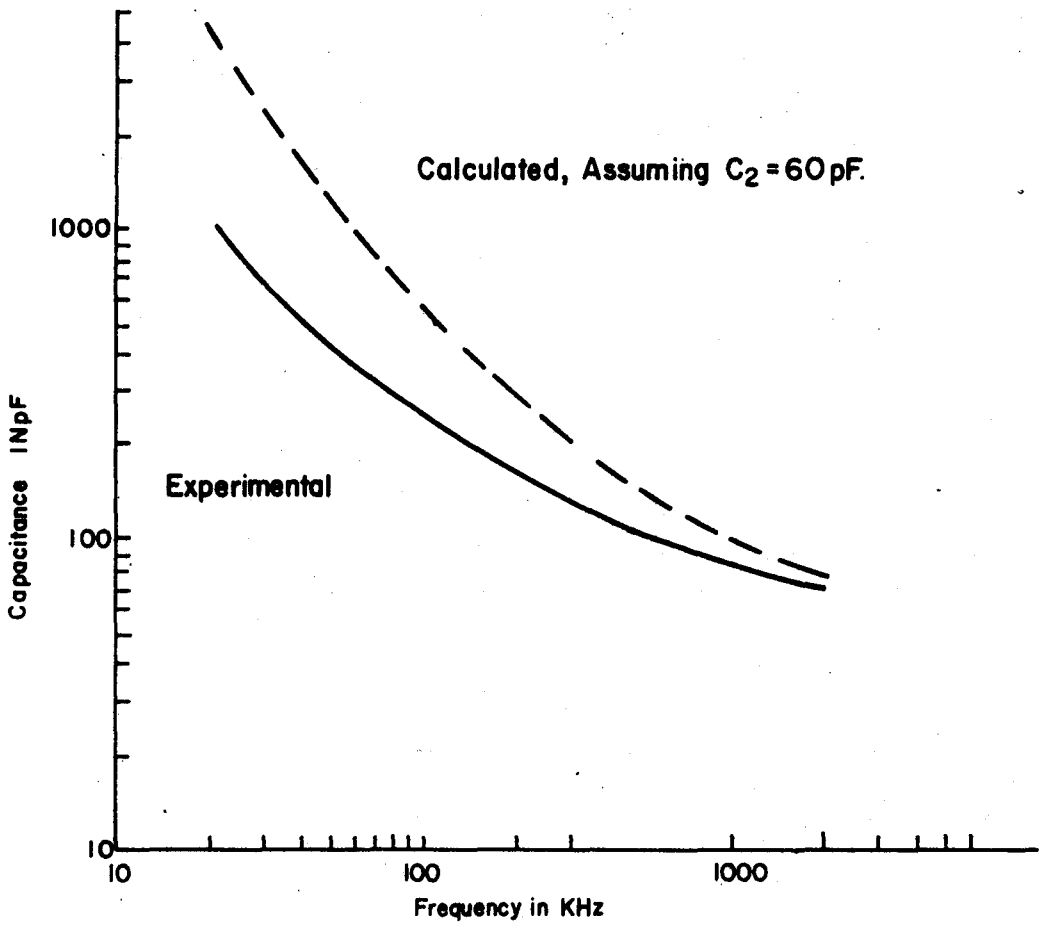

Figure 6. Capacitance of a coaxial sample holder loaded with Crider clay (42.8% moisture) as a function of frequency. Empty holder capacitance assumed to be 60pF.

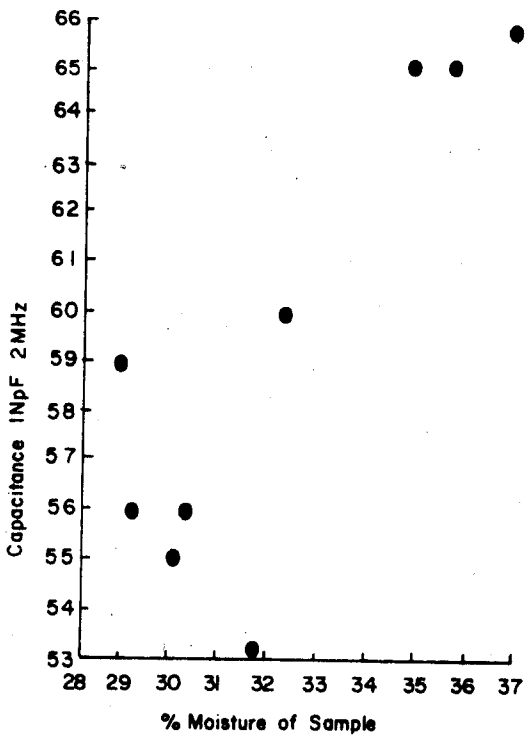

Figure 7. Capacitance of a coaxial sample holder loaded with Crider clay as a function of moisture content. Measurement frequency, 2MHz.

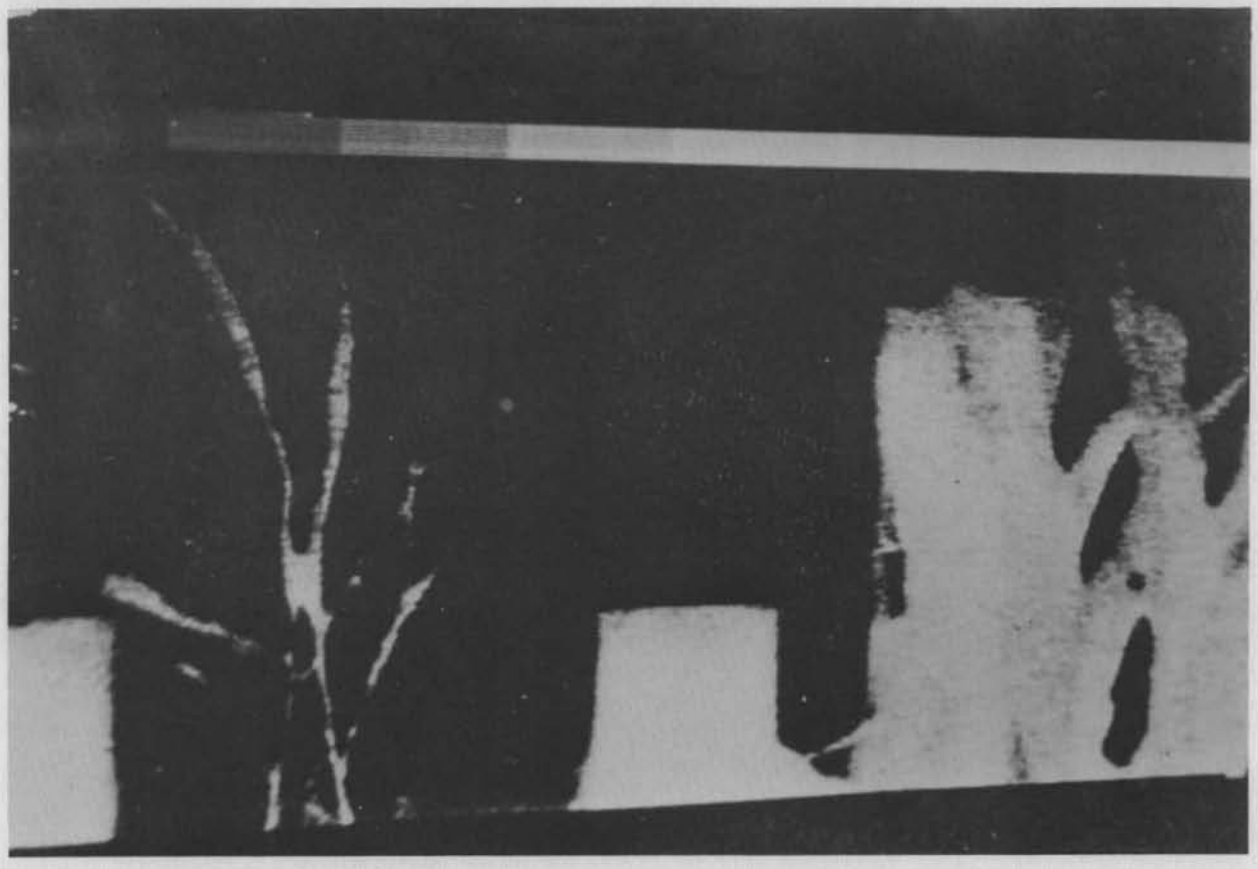

Figure 8. Thermogram of a sulfur deficient corn plant (on the left) as compared to a healthy corn plant (on the right). Ambient temperature is 24°C. A background behind the plants is at 16.5°C. The nutritionally stressed plant is approximately 1°C cooler than the healthy plant. Scan time: 6 minutes.

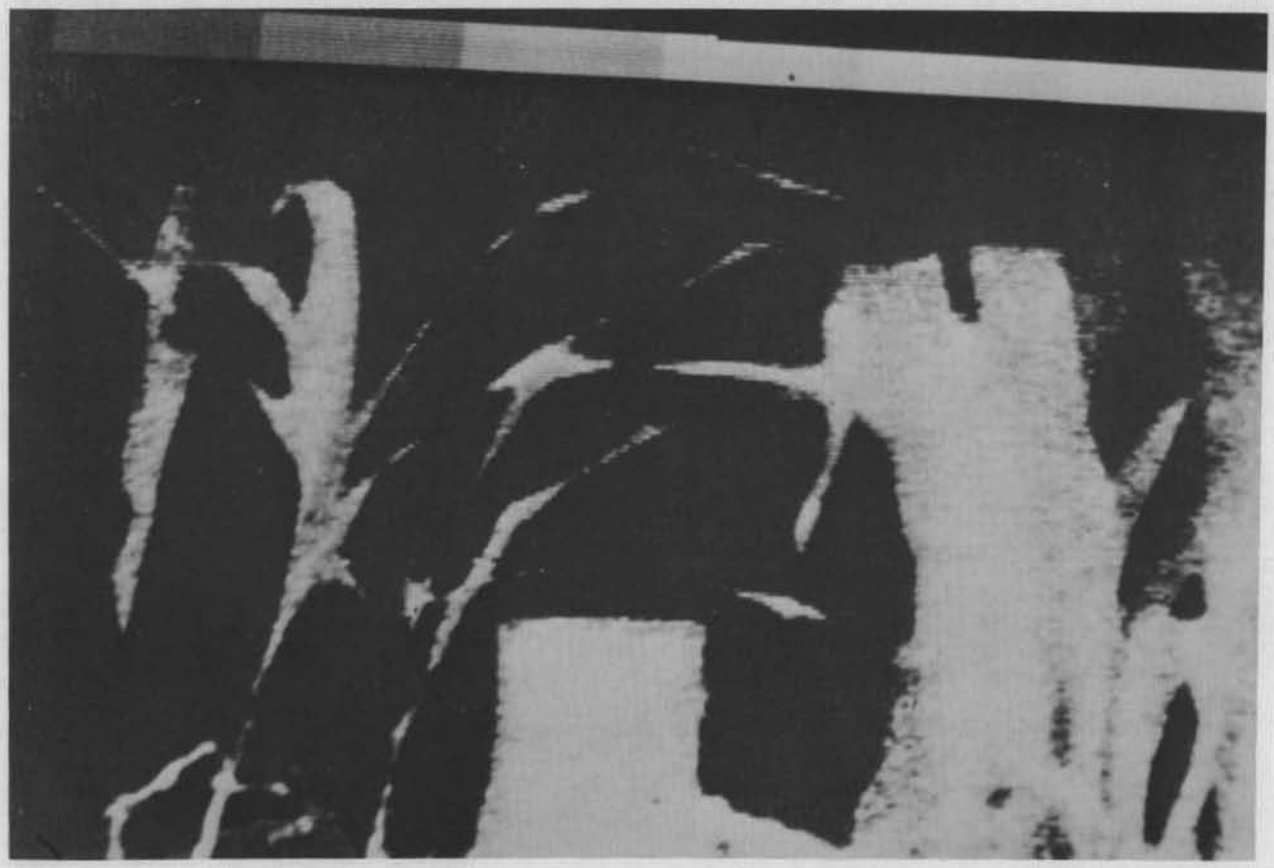

Figure 9. Thermogram of a nitrogen deficient corn plant (on the left) as compared to a healthy corn plant (on the right). Ambient temperature is 24°C. A background behind the plants is at 16.5°C. The nutritionally stressed plant is approximately 2°C cooler than the healthy plant. Scan time: 6 minutes.

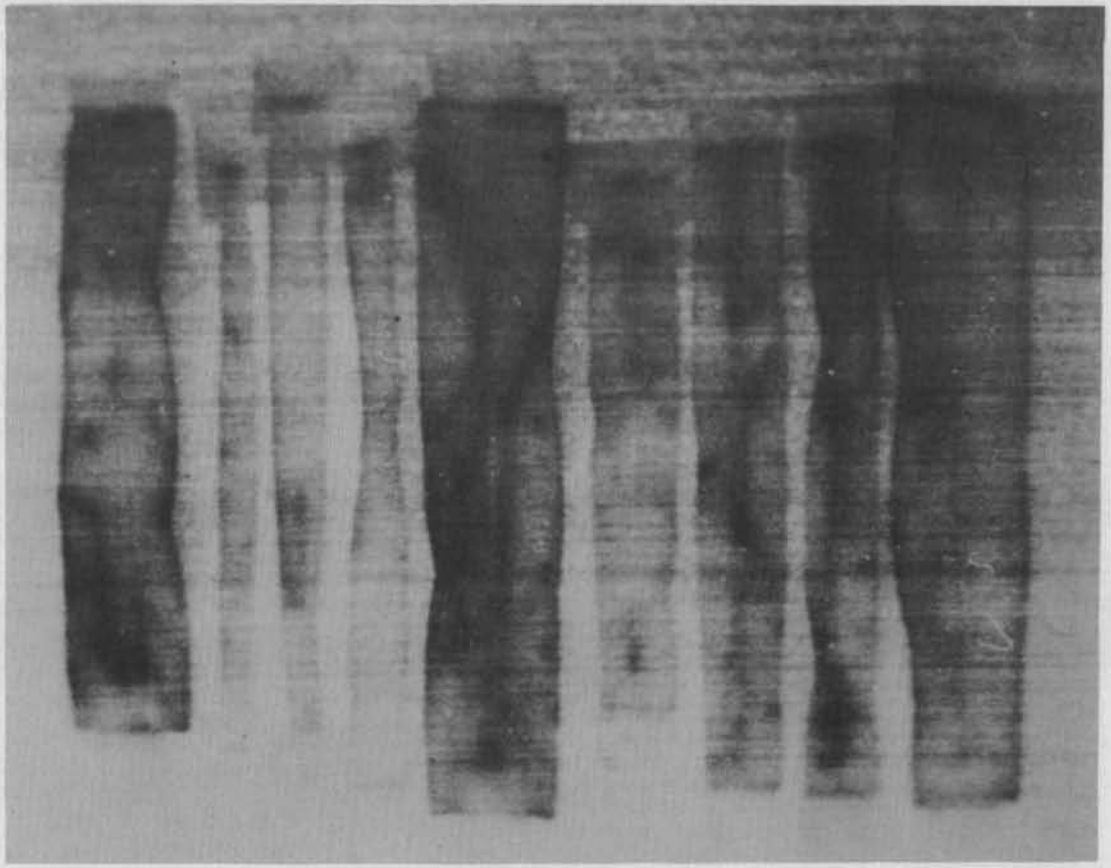

Figure 10. A thermogram of healthy and nutritionally stressed corn leaves. From left to right: healthy, three sulfur deficient, healthy, three nitrogen deficient, healthy, styrofoam background. Ambient temperature is 23°C but a 35°C surface is located nearby. The sulfur deficient leaves are approximately 1°C warmer and the nitrogen deficient leaves are approximately 2°C warmer than the healthy leaves.

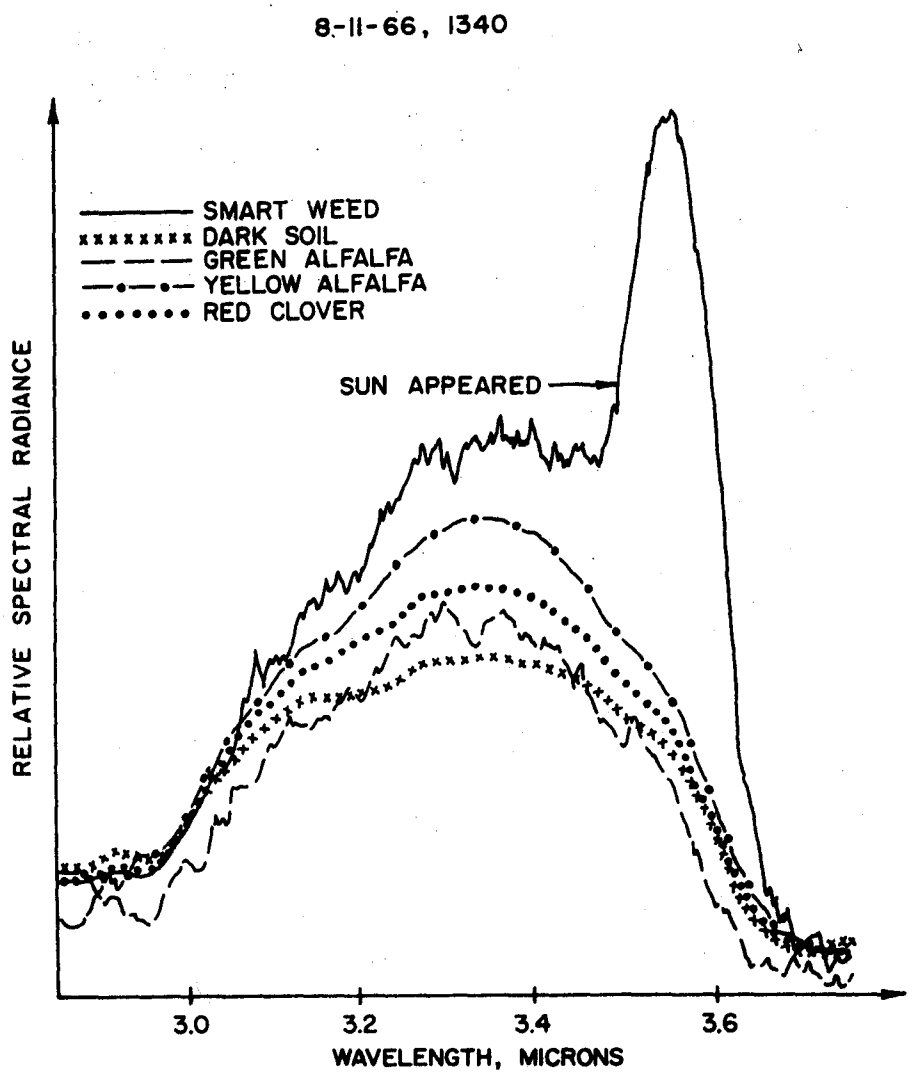

Figure 11. Spectral data taken with a Perkin-Elmer SG-4 spectroradiometer on a variety of cover types. The relatively long spectral scan time of the instrument permits environmental changes to compromise the data.

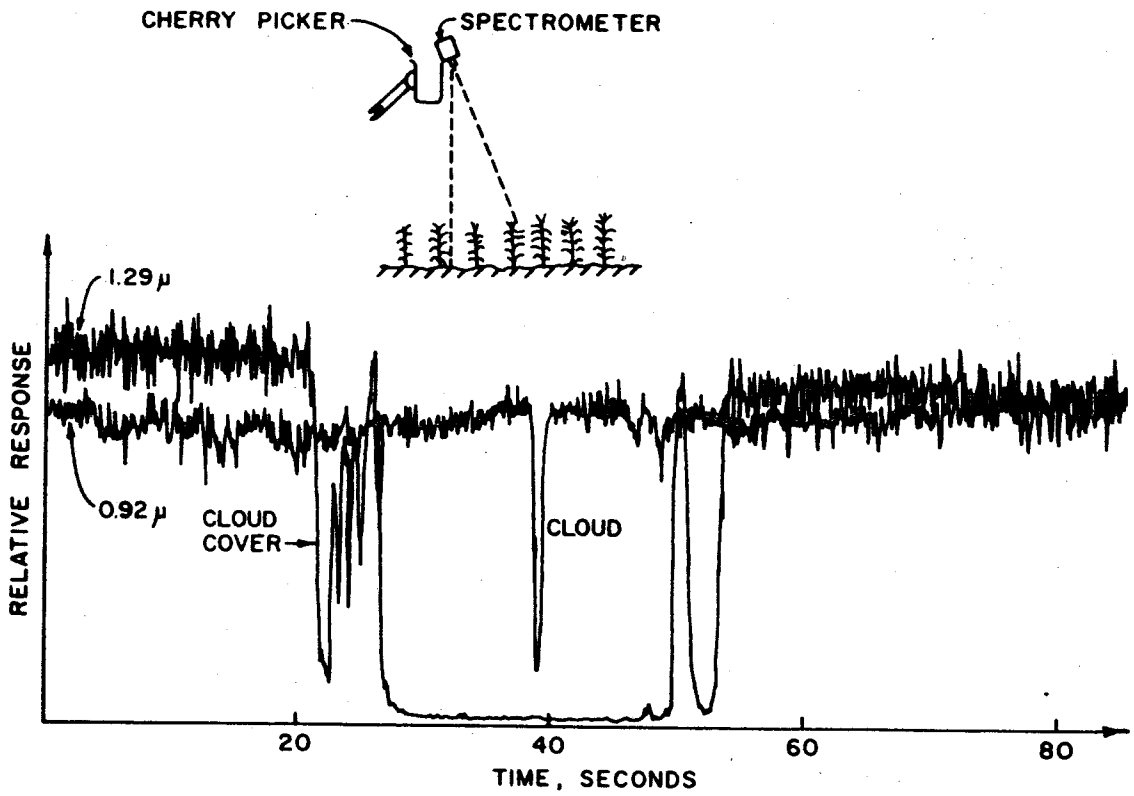

Figure 12. Radiometric data obtained by stopping the Perkin-Elmer SG-4 spectroradiometer at two fixed wavelength positions. The "noise" in the data is due to plant motion, not detector noise.

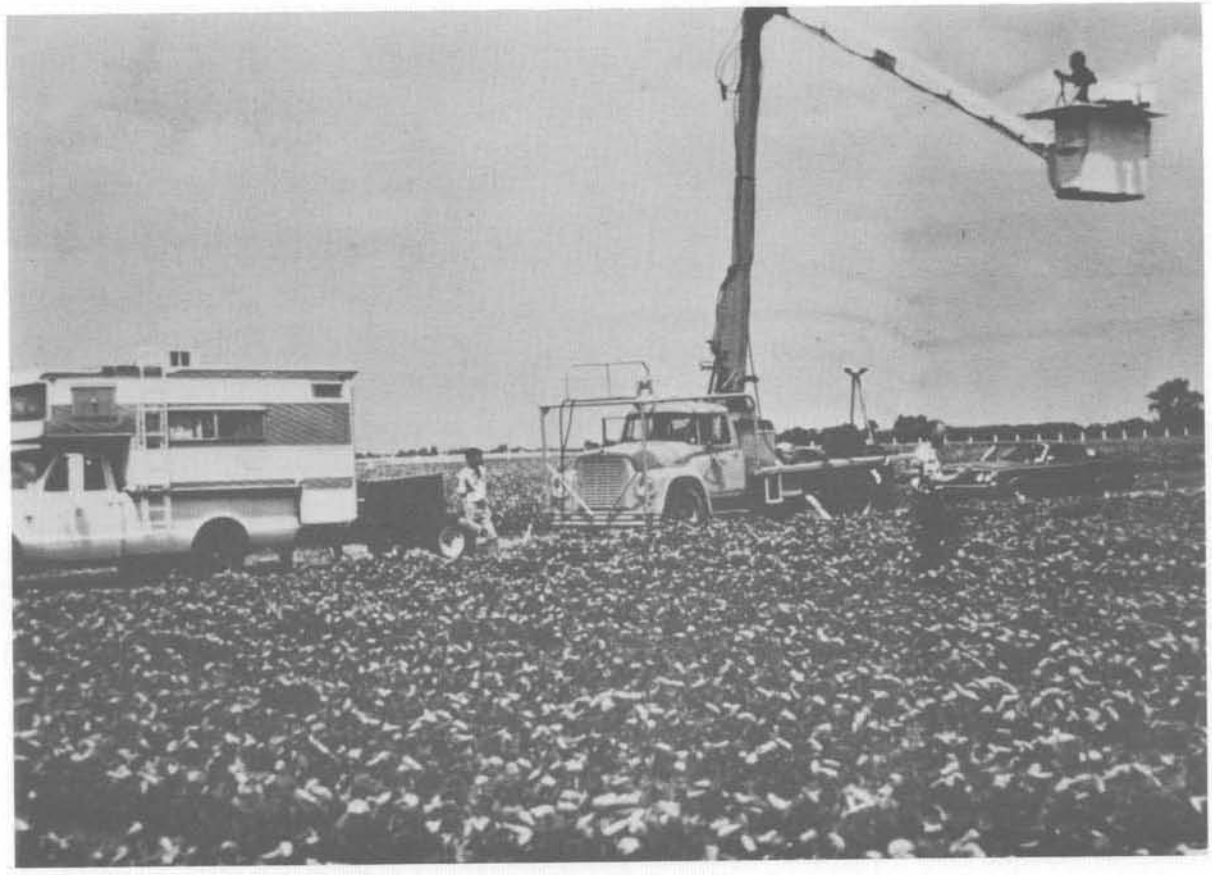

Figure 13. The Exotech Model 20B spectroradiometer undergoing field trials.

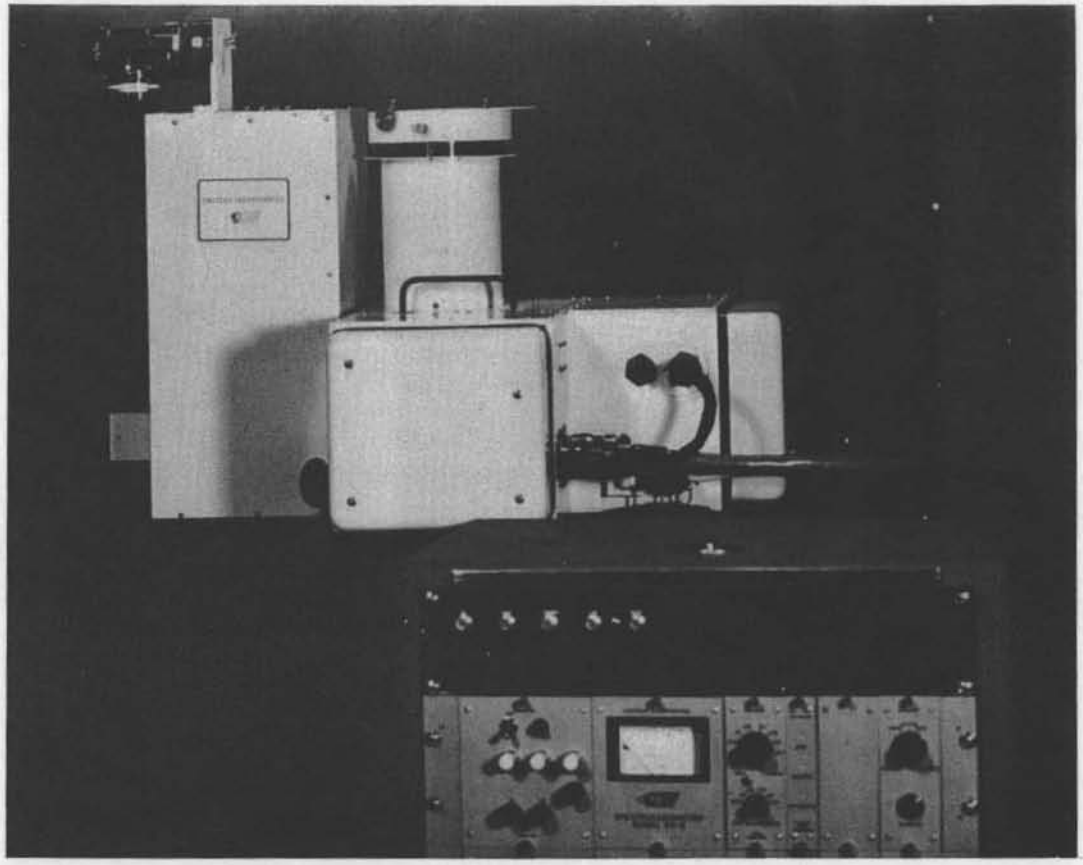

Figure 14. A general view of the Model 20C spectroradiometer short wavelength unit showing the control panel.

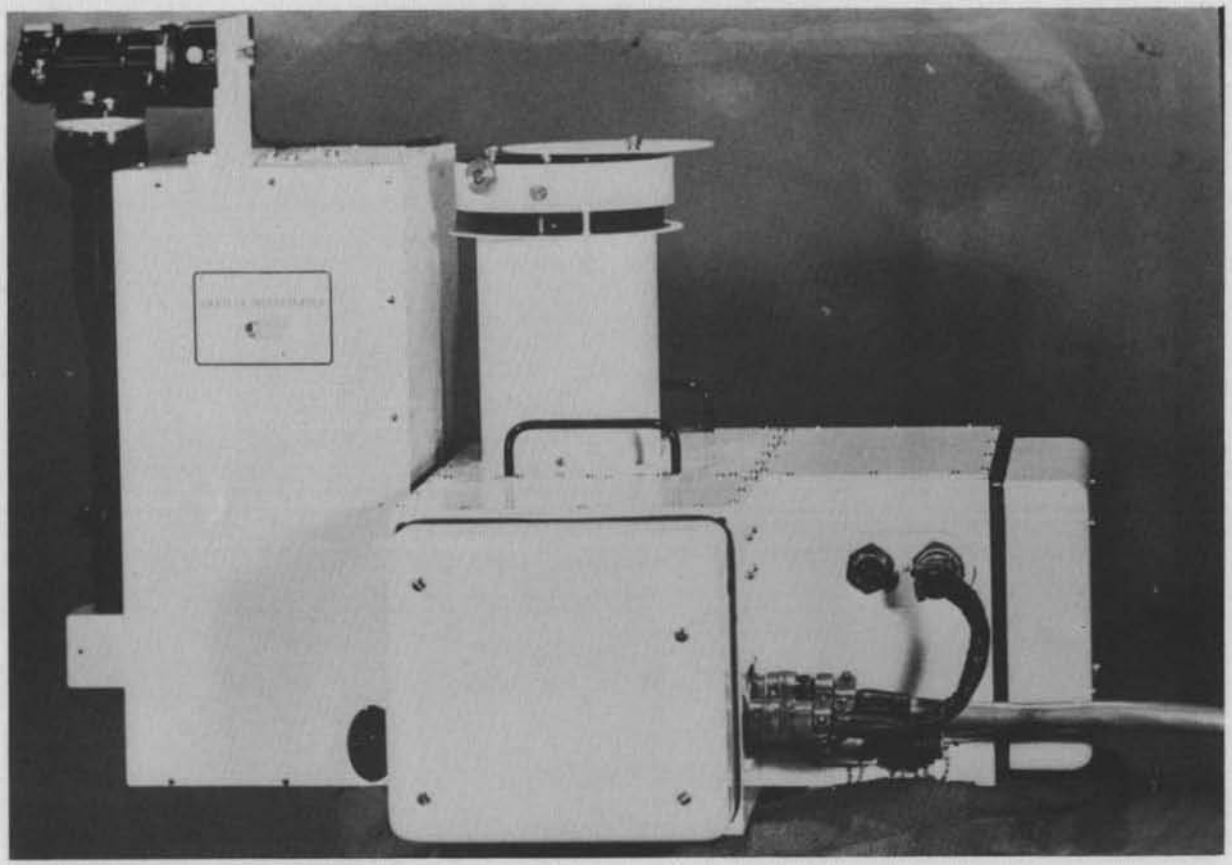

Figure 15. A close-up view of the Model 20C short wavelength head. The vertical tube is the solar irradiance input port.

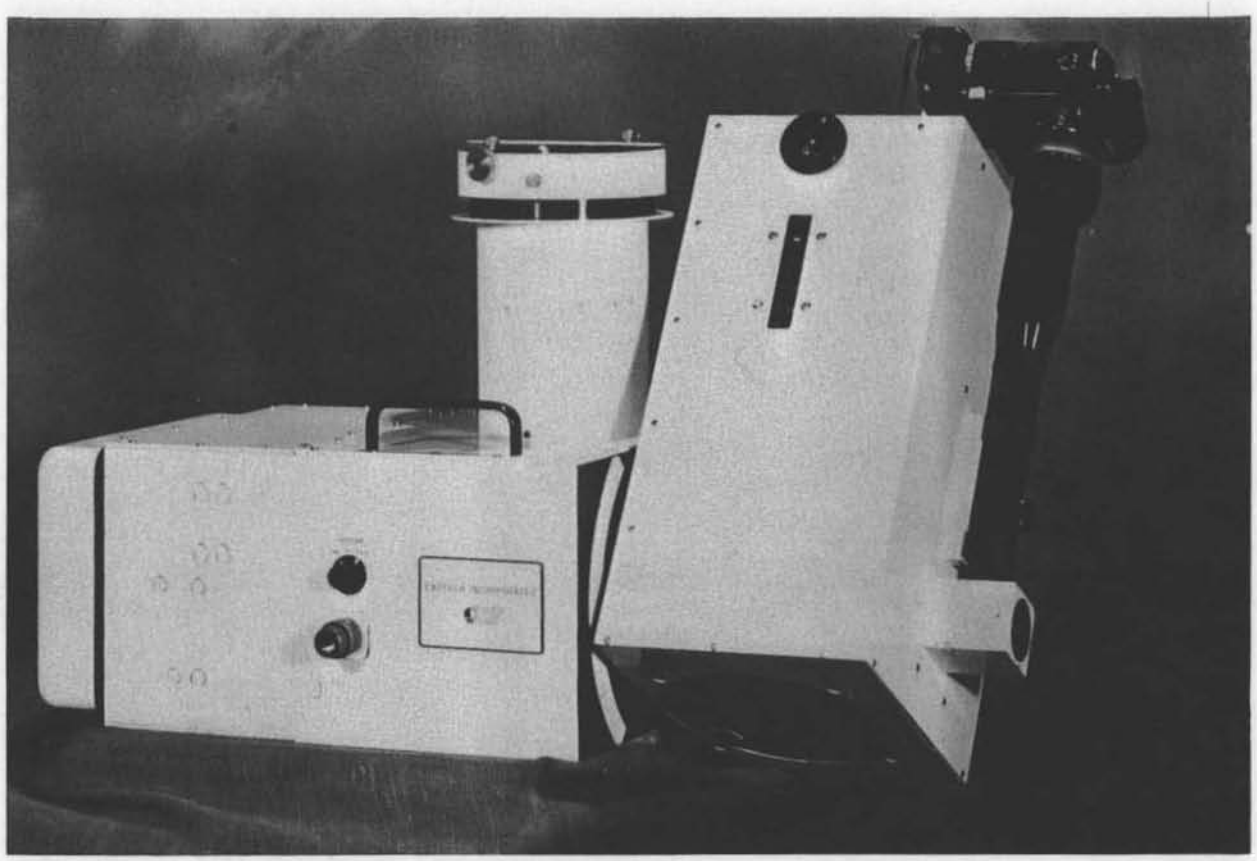

Figure 16. The view angle adjustment feature of the Model 20C spectroradiometer.

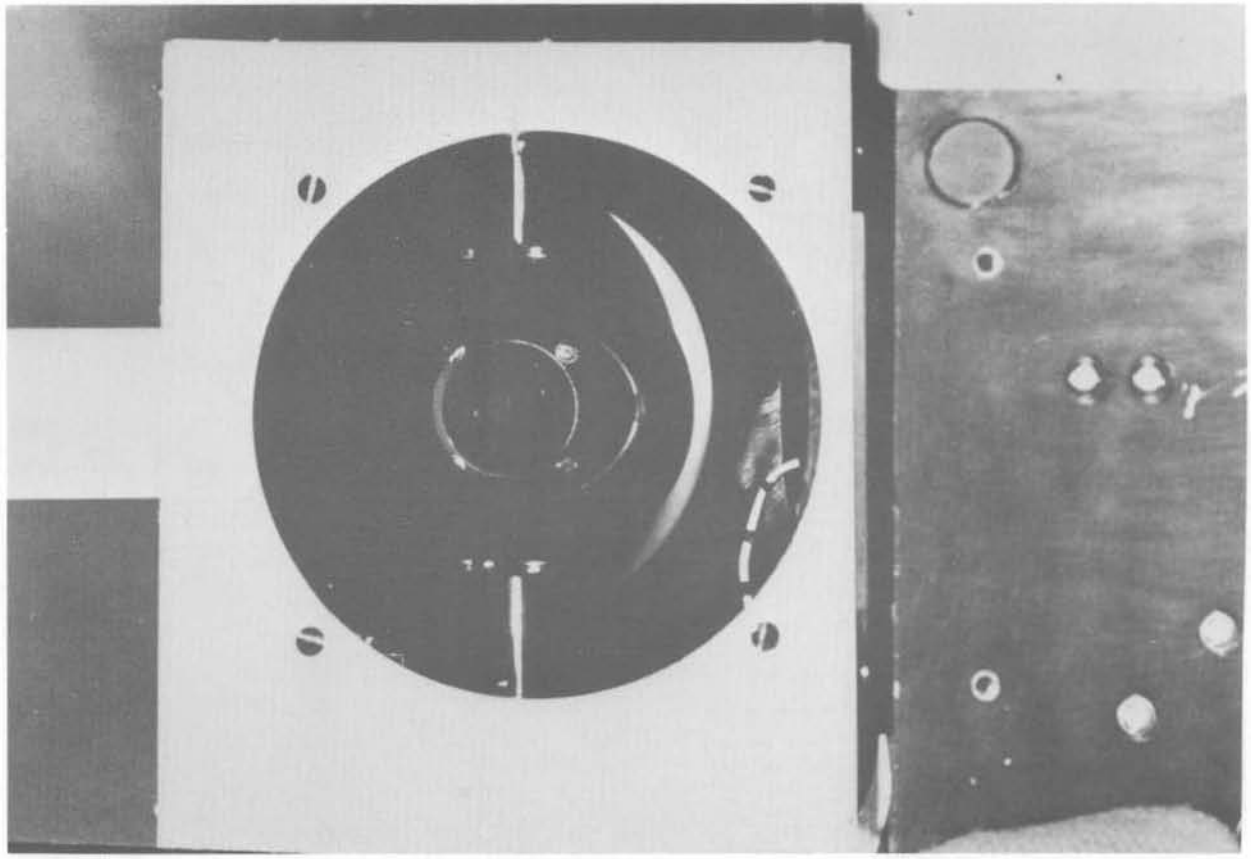

Figure 17. A view into the Newtonian fore-optical telescope of the Model 20C.

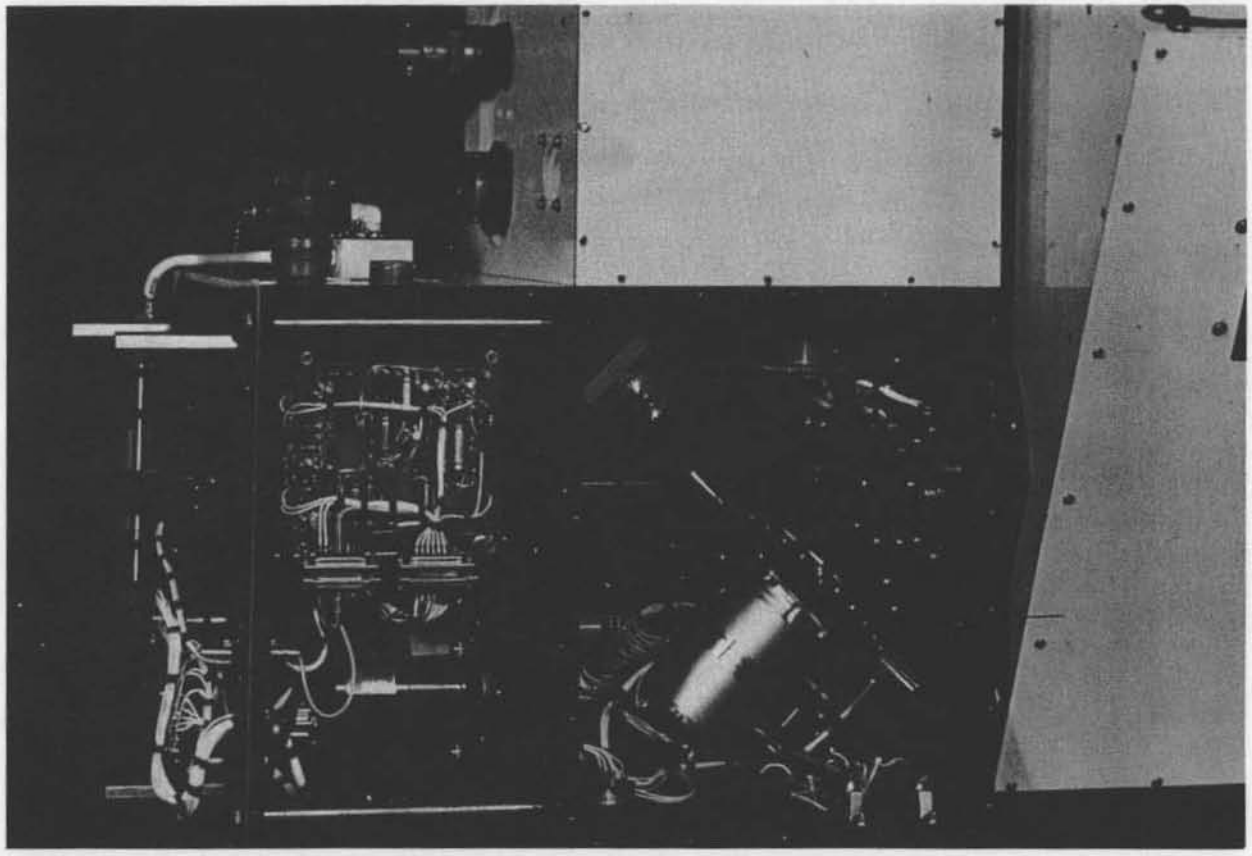

Figure 18. The internal structure of the Model 20C spectroradiometer. The chopper wheel is visible in the middle of the main compartment. Also shown is the filter wheel drive system and relay optical system.

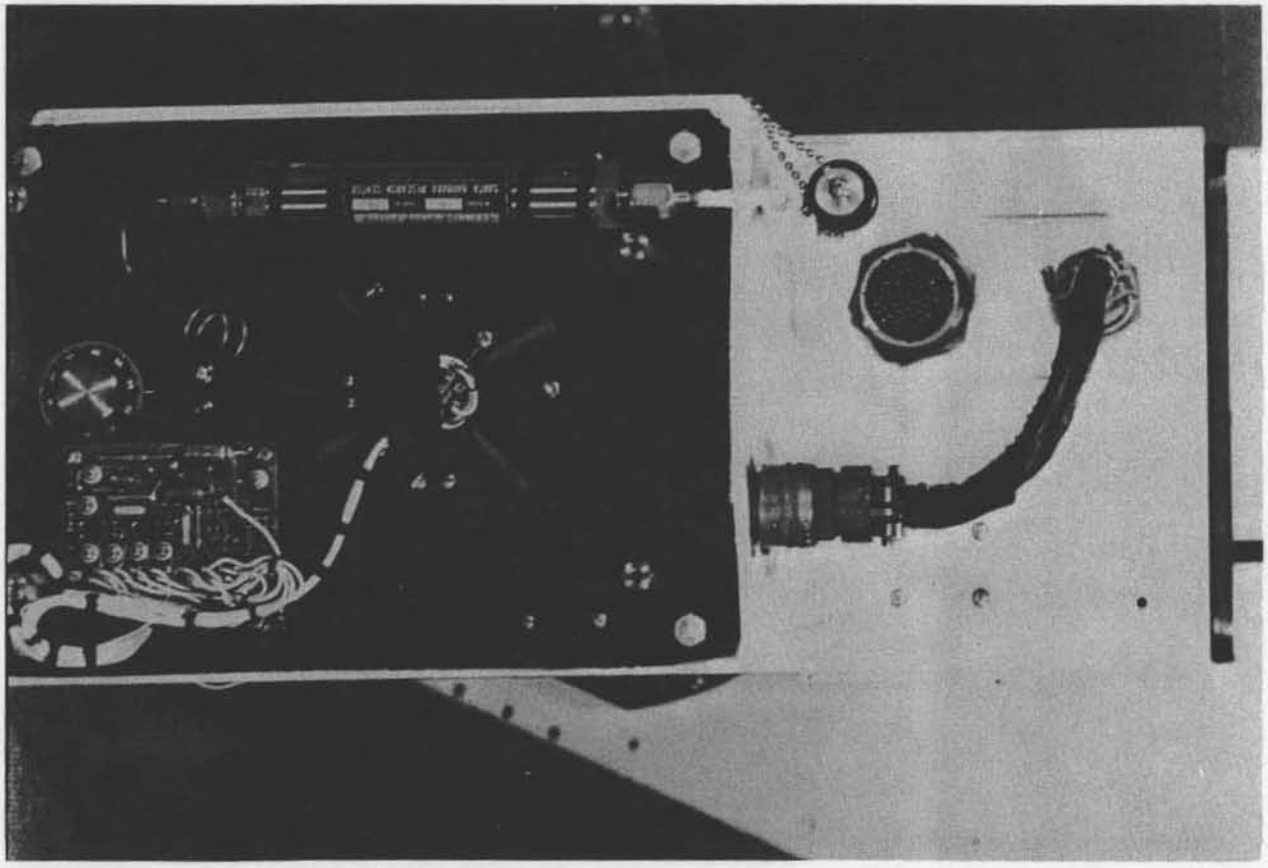

Figure 19. A view of the Joule-Thompson cooling system on the lead-sulfide detector of the Model 20C.

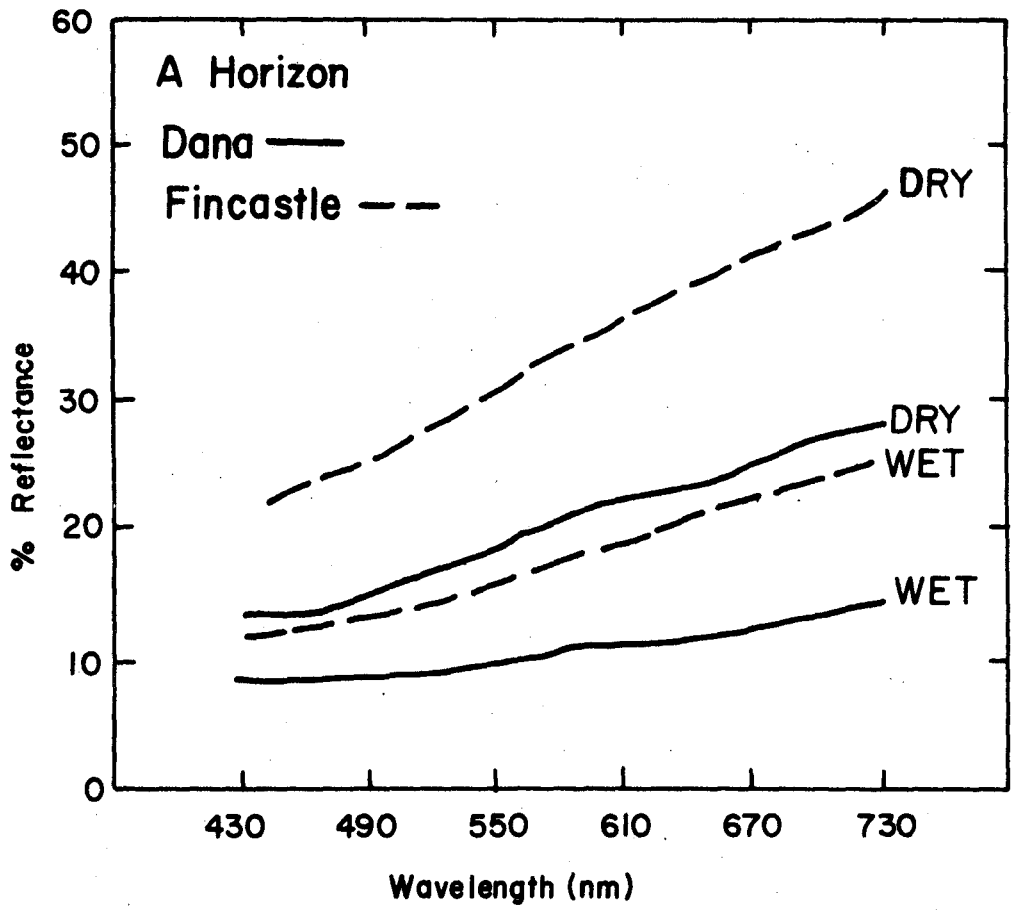

Figure 20. Soil spectral reflectance field, data obtained on the Model 20B spectroradiometer. The data were reduced manually.

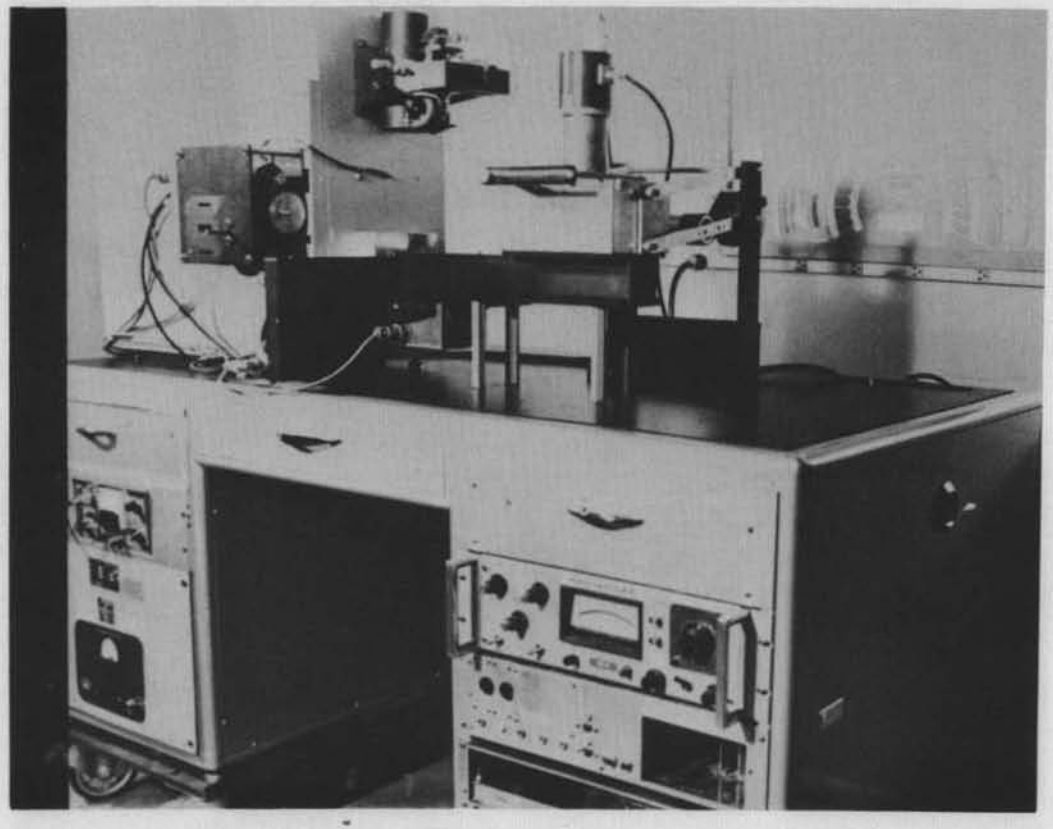

Figure 21. A general view of a large sample high-power, biological spectrophotometer.

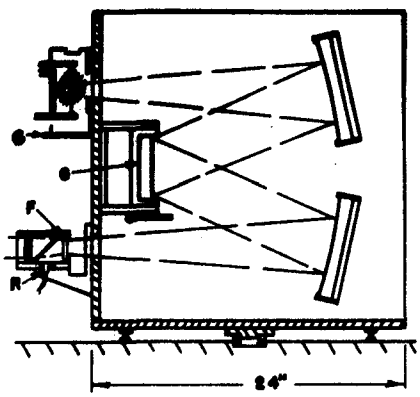

Figure 22. A schematic diagram of the biological spectrophotometer monochromator assembly.

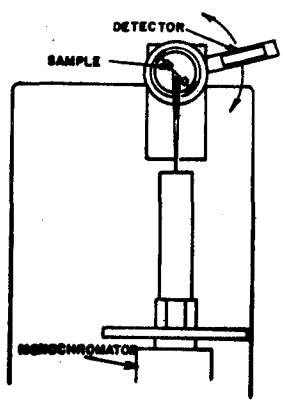

Figure 23. The bi-direction reflectance attachment for the spectrophotometer.

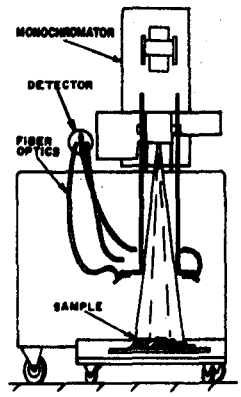

Figure 24. The large area reflectance attachment for the spectrophotometer.

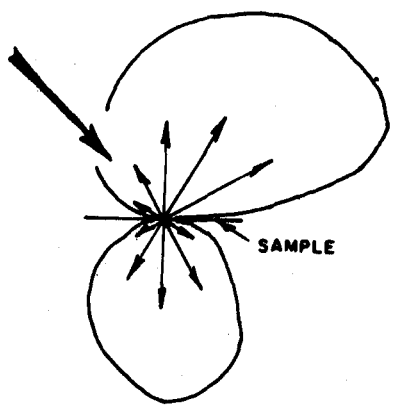

Figure 25. Typical bi-directional reflectance data for natural specimens.